

Article

Broadband Spectral Amplitude Control in High-Order Harmonic Generation

Carles Serrat

UPC-Polytechnic University of Catalonia, Colom 11, 08222 Terrassa (Barcelona), Spain;
E-Mail: carles.serrat-jurado@upc.edu; Tel.: +34-93-7398137; Fax: +34-93-7398000

Received: 26 October 2012; in revised form: 1 December 2012 / Accepted: 7 December 2012 /
Published: 19 December 2012

Abstract: A technique for broadband spectral amplitude control of light pulses produced in high-order harmonic generation (HHG) is presented. It has been shown elsewhere that broadband spectral phase control in HHG is achievable using a computerized feedback loop scheme by coherently adding a filtered region of the HHG emission to the intense IR driving pulse with optimal attenuation and time delay parameters. In the present study, further computational evidence of the capabilities of this control scheme is provided by considering the spectral amplitude in a broadband region of the HHG spectrum as the control target for the production of isolated attosecond pulses. Different spectral widths and central photon energies are examined, such as a spectral width of 30 eV centered at 36 eV, well in the plateau, and a width of 20 eV centered at 60 eV in the cutoff region. An iterative procedure of the method is implemented and optimal isolated single cycle pulses at a central photon energy of 36 eV are obtained. This control scheme is a fundamental tool that can be implemented for amplitude and phase shaping of any suitable spectral region in HHG.

Keywords: ultrashort pulses; attosecond pulses; coherent control; high-order harmonic generation; strong field

1. Introduction

A method for controlling the spectral phase and amplitude of broadband coherent light from high-order harmonic generation (HHG) is presented. The method considers a feedback loop scheme [1] and takes advantage from the coherent emission in HHG. Controlling the phase and amplitude of a broad spectral region in HHG represents a formidable challenge of general implication to many areas of

science [2]. In particular, the shaping of the phase and amplitude in a broadband is an essential ingredient for the reconstruction of the time profile of attosecond pulses.

It is well known that the broadband emission from HHG is a source for coherent attosecond light pulses, which can span photon energies from the ultraviolet to the soft X-ray region [3]. Controlling the amplitude and phase of the harmonic radiation is crucial to produce pulses with a duration as short as the bandwidth of the generated radiation in principle allows and to isolate them by compressing the energy generally delivered as pulse trains from the HHG process. Isolated attosecond pulses have demonstrated a great potential in the investigation of ultrafast electronic processes, and they can be produced by spectral selection of the few harmonics in the cutoff region, which are most in phase [4–6]. Several other techniques have been investigated to generate isolated and twin-pulses [7–19], which include spectral amplitude and phase control by means of polarization and intensity modulation of the driving pulses [7–12], the use of dispersive elements for pulse compression [13], and different other techniques [14–16] that have been reviewed in [18,19]. These important efforts are able or promising to produce isolated attosecond pulses by considering a particular spectral bandwidth of the harmonics spectrum. The feedback loop control presented here allows to directly control the HHG process such that the light is emitted with the desired shape from any chosen spectral bandwidth of the harmonics spectrum. As it will be shown, this technique is very robust in particular for the production of isolated attosecond pulses.

In a recent work [20], it has been shown that the spectral phase of the emission from HHG can be directly manipulated in any suitable broad spectral region by considering the coherent addition of a filtered spectral width of the HHG spectrum, with optimal delay and attenuated intensity, to the strong IR input pulse. This procedure is controlled by a numerical algorithm and allows to optimally shape a broadband spectral phase, so that isolated attosecond pulses can be produced from different bandwidths of the spectrum and at different central photon energies. In the present work, this control technique is further examined by considering the spectral amplitude of the HHG spectrum as an alternative control target in the optimization procedure. As it will be shown, by flattening the shape of the spectral amplitude in a large bandwidth of the harmonics spectrum, isolated attosecond pulses are produced, which provides a significant example of HHG broadband amplitude control. The present results therefore extend the capabilities of the HHG control technique first described in [20].

As mentioned above, the feedback loop is based on using a filtered spectral width of the HHG spectrum to slightly reshape the HHG driving pulse, which is accomplished by a coherent combination of a weak XUV pulse with the strong IR driving field. Combining attosecond XUV pulses with the driving IR field has been studied for HHG [21–27], although the possibility to shape the amplitude and phase of a broad region of the spectrum by combining a weak XUV pulse with the intense IR driving pulse has not been considered before. The present results show that the spectral amplitude of the emission from HHG can be directly manipulated in a broad spectral region—as it was demonstrated by considering the spectral phase in [20], to provide an optimal amplitude shape for the production of isolated attosecond pulses. By considering different significant examples, it is shown how this technique can be implemented, in principle, for any suitable region of the harmonics spectrum.

2. Experimental Section

The control technique basically includes a variable intensity attenuator, a variable delay line and a spectrum analyzer, which are managed by a computer. The experimental realization is limited by the existence of the optical elements at the different bandwidths and photon energies that are of interest. In this respect, the present work attempts to demonstrate the feasibility of the control method by analyzing different significant examples, since the observed effect cannot be addressed in general due to the intrinsic characteristics of a coherent control tool based on feedback loop schemes. Otherwise, the observed results are based on a conceptually clear physical mechanism. The manipulation of the spectral amplitude/phase of the harmonics is based on the coherent combination of several harmonic generation zones with appropriate delays in between and with optimal intensities, such that the resulting spectral amplitude/phase is modified in a broad spectral region, or equivalently, the addition of a weak filtered region of the emitted spectrum to the IR intense driving pulse produces a small reshape of the IR field that conveniently modifies the amplitude and phase of the electron quantum trajectories generating the different photon energies in the HHG process.

As schematically illustrated in Figure 1, a 5 fs laser pulse with Gaussian temporal profile, carrier-envelope phase CEP = 0°, central wavelength of 800 nm and peak intensity of 2×10^{14} W/cm² interacts with a gas medium—helium in the present simulations (ionization potential 24.59 eV), producing high-order harmonics with a photon energy cutoff at ≈ 70 eV. In the present study, the considered feedback loop scheme evolves as follows: a first spectral filter selects the desired bandwidth of the generated radiation in the XUV region that is to be optimized. The energy of this XUV₁ pulse is modified by a variable light attenuator (A₁) that scans for optimal intensities, and then it passes through a variable delay line (D₁) that scans for the position with respect to the IR pulse where the XUV₁ pulse is to be added. Coherently combined, the resulting IR + XUV₁ pulse is then sent to a second helium gas target that produces a second high-order harmonics signal. The output from the second gas target is filtered to select the same bandwidth as in the first interaction region, and the spectral amplitude of this last generated XUV pulse is reconstructed by using a spectrum analyzer. The information of the spectrum is then examined by a numerical algorithm that performs a linear regression from the data of the spectral amplitude versus photon energy and calculates its normalized chi-square (χ^2) function, such that the *flattest* spectral amplitude can be selected.

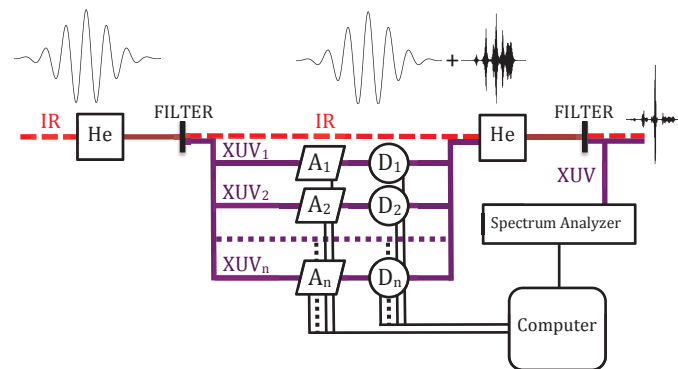
Hence, the problem of fitting a set of N data points (x_i, y_i) to a straight-line model $y = a + bx$ is considered, and the χ^2 function is used to measure how well the model agrees with the data. The χ^2 function is defined here as

$$\chi^2(a, b) = \sum_{i=1}^N (y_i - a - bx_i)^2 \quad (1)$$

The distance from each data point to the straight-line model is minimized by varying the parameters a and b in the sum of the squared distances between the data points and the estimate obtained from the function $y(x)$, which is often called a least squares fit [28]. If the straight-line passes through all the data points, the χ^2 function will obviously be zero and the fit is perfect. Due to the evident deviations of the spectral amplitude shape from the straight line this will not happen, and the numerical algorithm will thus find the parameters a and b that minimize χ^2 . A linear regression and a value of χ^2 is computed for

each intensity and position of the XUV₁ pulse, and after normalizing χ^2 with $\sum_{i=1}^N (y_i - \langle y \rangle)^2$ in each case, where $\langle y \rangle = \sum_{i=1}^N y_i / N$, the minimum normalized χ^2 value provides the combination of IR and XUV₁ pulses that produce the flattest spectral amplitude, *i.e.*, the closest to a straight-line. The method can readily be iterated by splitting the XUV pulse from the first gas target (XUV₁, XUV₂, ..., XUV_n, see Figure 1), so that an optimal driving pulse can be obtained iteratively resulting in some cases in an improved result, as it will be detailed below.

Figure 1. (Color online) Schematic illustration of the numerical experiment. An intense IR laser pulse interacts with a first gas target—helium in this case. The output is filtered in a particular spectral region—and occasionally split in several pulses, in order to modify the XUV intensity, which is achieved by using variable light attenuators A_i . The attenuated XUV_{*i*} pulses are combined with the original IR pulse with a given delay provided by variable delay lines D_i . The combination of the IR+XUV_{*i*} pulses generates harmonics in a second gas target. The output from the second interaction region is analyzed by a spectrum analyzer for optimization of the spectral amplitude in an iterative loop procedure managed by a computer.



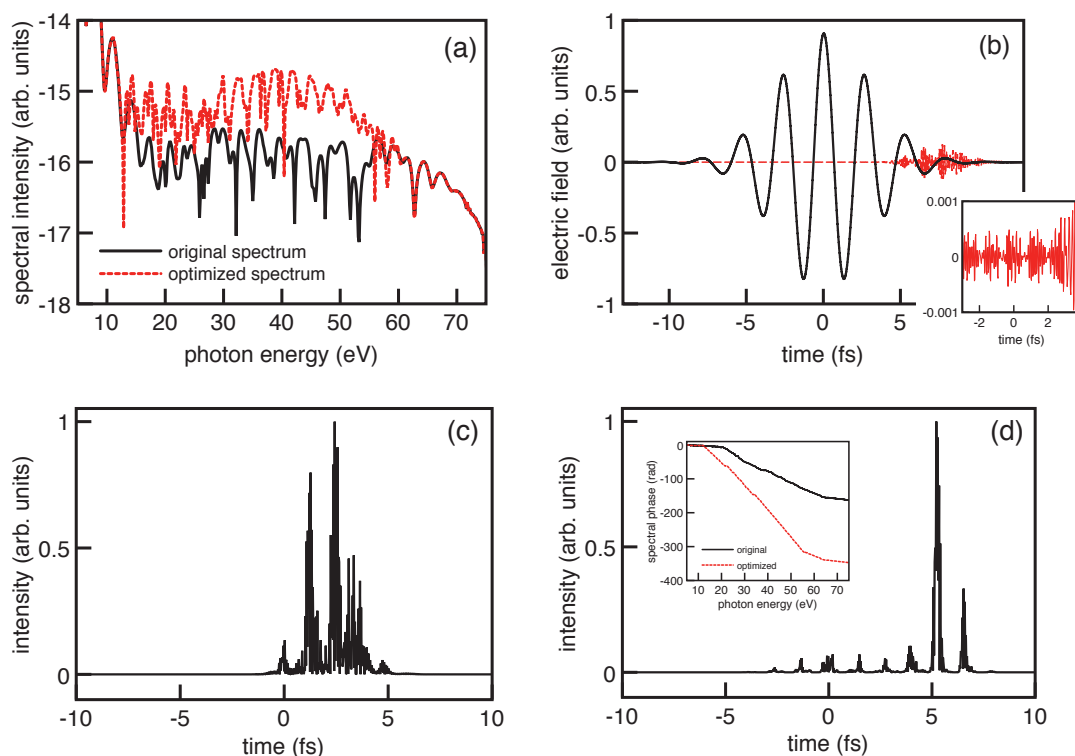
The simulations have been performed by numerically solving the atomic response in the single-atom non-adiabatic strong-field approximation [29] in order to demonstrate the control mechanism in the simplest case. Propagation effects can be important and their influence will be studied in a future extension of the work. Therefore, the present results apply for low-pressure HHG processes and for short propagation lengths.

3. Results and Discussion

In Figure 2 the optimization has been obtained by filtering the harmonics in a spectral region centered at 36 eV and considering a bandwidth of 30 eV, using a single loop iteration. The XUV₁ pulse resulting from the first gas target is combined with the IR intense pulse and sent to the second interaction region by scanning its intensity from $\alpha = 10^6$ to $\alpha = 10^7$, in steps of $\Delta\alpha = 10^6$, where α is an attenuation coefficient that has been defined with respect to the peak intensity of the IR pulse as $I_{XUV} = I_{IR}/\alpha$, with I_{XUV} and I_{IR} being the peak intensities of the XUV and the IR pulses, respectively. The position at which the XUV₁ pulse is combined with the IR pulse has been scanned from $\theta = -720^\circ$ to $\theta = 720^\circ$, in steps of $\Delta\theta = 2^\circ$, where θ is the angular location defined with respect to the IR cycle. From Figure 2a, we can observe that the obtained optimal spectral amplitude (red dotted line) is substantially enhanced

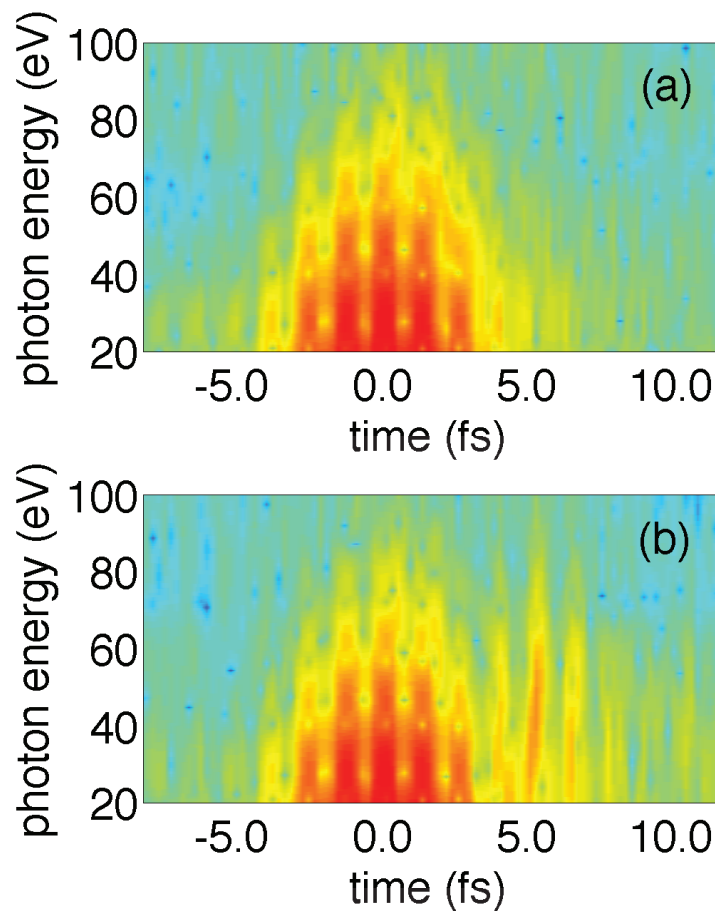
with respect to the original spectrum (black line), although the optimal XUV₁ pulse corresponds to an attenuation parameter as high as $\alpha = 10^7$. As commented above, the fitness function considered for the spectral amplitude control is the normalized χ^2 function obtained from a linear regression of the spectral amplitude versus photon energy in the second interaction region. The normalized χ^2 parameter is minimized by the numerical algorithm in order to find the values of the attenuation α and delay θ fitness parameters that produce a spectral amplitude shape the closest to a straight-line. The present results demonstrate that the fitness function χ^2 is indeed extremely efficient to achieve optimal isolated attosecond pulses by spectral amplitude shaping. As it can be observed from Figure 2c,d, the energy from the original HHG process is strongly compressed in time by the effect of the optimization process, which results in an almost single attosecond pulse, as shown in Figure 2d.

Figure 2. (Color online) Optimization of the HHG spectral region 21–51 eV obtained by considering a single feedback loop. The scan in θ is from $\theta = -720^\circ$ to $\theta = 720^\circ$, and α is scanned from $\alpha = 10^6$ to $\alpha = 10^7$. The value of the normalized χ^2 function is 0.9998 for the original spectrum and 0.8929 for the optimized one. In (a) the spectral intensity of the original and optimized spectra are shown, as indicated. The IR driving pulse together with the optimal XUV₁ pulse are shown in (b). The amplitude of the IR pulse is normalized, and the one corresponding to the XUV₁ pulse has been rescaled to allow its visualization. In this case the optimal values of the fitness parameters are $\alpha = 10^7$ and $\theta = 718^\circ$. (c) and (d) show the temporal evolution of the intensities of the XUV pulses resulting from the second interaction region, before and after optimization, respectively, which are centered at a photon energy of 36 eV. The inset in (d) shows the spectral phase for the original and optimized spectra. Note that the labels in the vertical axis of (a) indicate a logarithmic scale.



The physical mechanism by which the optimal pulse is achieved, and in particular how much of the ionization in the process is due to tunneling, considering a tiny change in the electric field of the IR pulse, how much is due to ionization caused by the XUV₁ field, or by the effect of time modulation of the atomic potential and bound wave function is difficult to elucidate. However, some insight of the physics behind the described process can be obtained. Figure 2b shows how the optimal position at which the XUV₁ pulse is added lies in the temporal late wing of the IR pulse, which in this case corresponds to $\theta = 718^\circ$. Also, the inset in Figure 2b shows the amplitude of the XUV₁ pulse near the center of the IR pulse. Observing the reduction of the intensity generated in the HHG process from the central part of the IR pulse (Figure 2d), we can conclude that the small perturbations in the center of the IR pulse caused by the early wing of the XUV₁ pulse induce a phase reshaping in the HHG quantum trajectories that result in a strong cancellation of the HHG signal. This conjecture is supported by the fact that small variations on the amplitude of the IR field can produce a substantial change on the phase of the quantum trajectories, as it is described in detail in [20], and also by an analysis of the mostly contributing trajectories that will be shown below. In the present case we hence observe that a flattening of the spectral amplitude involves a synchronization of the phases in the quantum trajectories participating in the HHG process, so that the overall spectral phase results optimally changed. As it is shown in the inset of Figure 2d, the spectral phase of the spectrum is indeed substantially modified by the optimization process. As commented above, an additional insight on the contribution of the two main electron trajectories involved in the HHG generation process can be obtained by an study of the time distribution of the energy in the spectrum, which is shown in Figure 3. Although the resolution of the figure is not optimal due to limitations from the numerical simulations, the cycles in the photon energy versus time plane, which correspond to the time-dependent intensity profile of the IR pulse, can still be well recognized. Indeed, each cycle accords to half period of the driving IR pulse, with the earlier half of each cycle showing the first occurring recollisions (short trajectories) and the second half showing the contribution of the long trajectories. The duration of the two trajectories coincides in the cutoff, where the highest photon energies are generated. Only qualitative results are shown in Figure 3 for clarity, with a more intense red color indicating a higher harmonics yield. In Figure 3a the original unperturbed spectrum shows an obvious symmetry. The spectrum in Figure 3b, which corresponds to the optimized case, shows two important features: first, there is not a selection of a particular trajectory in the central part of the IR pulse, which supports that a destructive interference between the short and long trajectories is produced in this region due to variations in their relative phase. Second, the perturbation produced by the XUV₁ pulse in the late wing of the IR pulse induces an enhancement of the signal in the spectral region that is optimized (21–51 eV) together with a suppression of the contribution of the long trajectories in that region, which is a relevant consequence of the optimization procedure. The overall effect is a confinement of the HHG signal at ≈ 5 fs ahead from the peak of the IR pulse, which results in an almost isolated attosecond pulse (see Figure 2d).

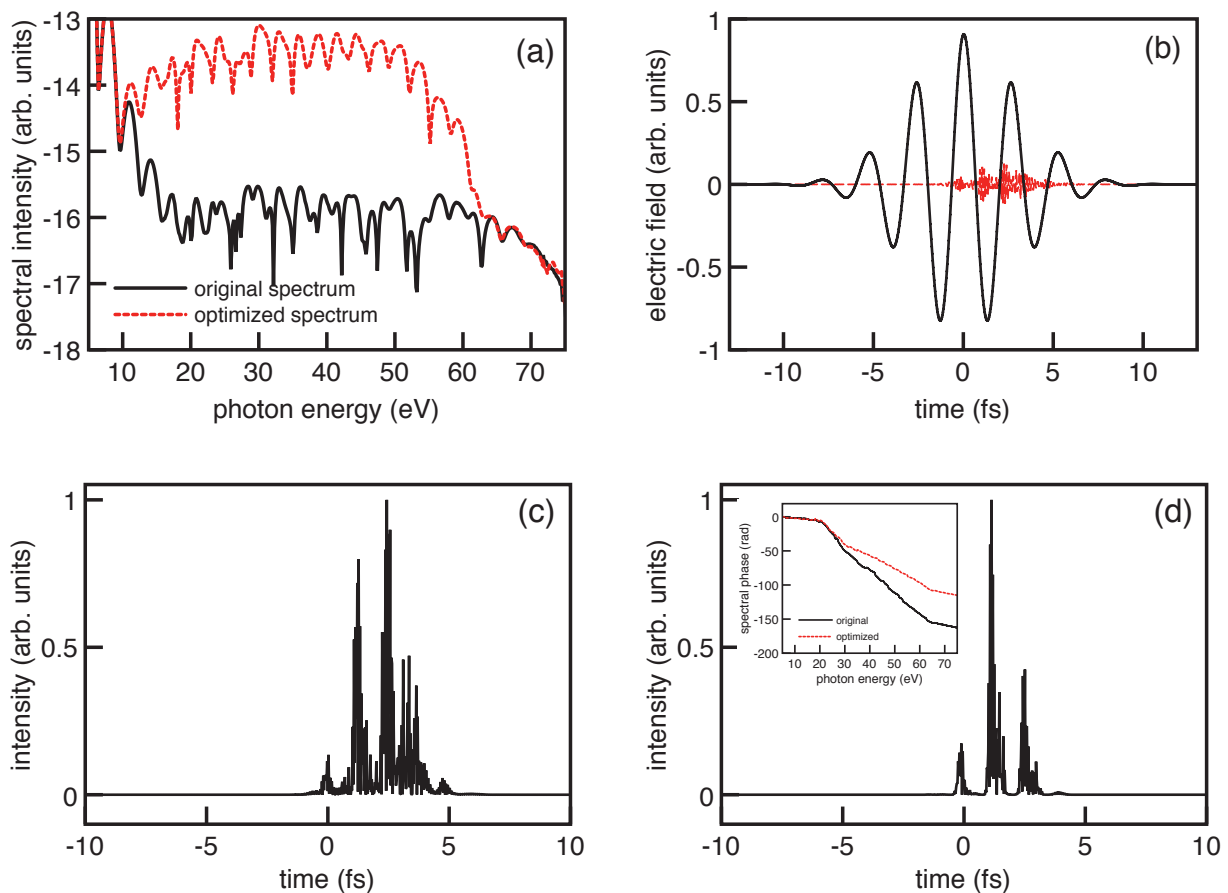
Figure 3. (Color online) Time-frequency analysis of the original (a) and optimized (b) spectra, for the case shown in Figure 2.



In order to investigate the influence of the position at which the attosecond XUV₁ pulse is added with respect to the IR driving field on the optimization procedure, the previous simulations have been repeated by allowing the scan of the position angle θ to run only from $\theta = -180^\circ$ to $\theta = 180^\circ$, and by keeping the attenuation parameter fixed to $\alpha = 10^7$. As shown in Figure 4, an optimal angular position is found in this case at $\theta = -22^\circ$, which results in a perturbation of the IR driving pulse around the end of its first cycle (see Figure 4b). By comparing Figures 2a and 4a, it can be observed that the effect of the shift of the position of the XUV₁ pulse to the higher values of the IR electric field results in a higher enhancement of the optimal spectral amplitude with respect to the original spectrum. Also, since the value of the normalized fitness function χ^2 for the optimal spectrum is not as low in this case ($\chi^2 = 0.9893$) as it was in the previous simulations ($\chi^2 = 0.8929$), *i.e.*, the achieved spectrum is not as optimal, since the results in Figure 2 have been obtained by using a scan in θ that includes the region of the scan considered in Figure 4, the resulting compression in time of the output pulse is not as efficient as in the previous case, as it is clear by comparing Figure 2d with Figure 4d. The time-frequency analysis from this case is shown in Figure 5. We can observe again that the perturbation by the XUV₁ pulse in the optimal configuration induces a considerable suppression of the long trajectories in the enhanced region. Note that the suppression of the long trajectories is however not as complete in this case as it was in the

case of Figure 3, but it can still be observed in the photon energy region between 21 and 51 eV, in the 3 last mostly IR contributing cycles.

Figure 4. (Color online) Optimization of the HHG spectral region 21–51 eV obtained by considering a single feedback loop. The scan in θ is from $\theta = -180^\circ$ to $\theta = 180^\circ$, and α is fixed to 10^7 . The value of the normalized χ^2 function is 0.9998 for the original spectrum and 0.9893 for the optimized one. In (a) the spectral intensity of the original and optimized spectra are shown, as indicated. The IR driving pulse together with the optimal XUV pulse are shown in (b). The amplitude of the IR pulse is normalized, and the one corresponding to the XUV pulse has been rescaled to allow its visualization. The optimal value for the angular position results in $\theta = -22^\circ$. (c) and (d) show the temporal evolution of the intensities of the XUV pulses resulting from the second interaction region, before and after optimization, respectively, which are centered at a photon energy of 36 eV. The inset in (d) shows the spectral phase for the original and optimized spectra. Note that the labels in the vertical axis of (a) indicate a logarithmic scale.



The results shown in Figures 2 and 4 consider one iteration of the optimization procedure (see Figure 1). For a scan of the attenuation parameter such as the one that has been used ($10^6 < \alpha < 10^7$), no further optimization is observed in this case by considering additional iteration loops. In order to investigate the capabilities of the multiple iteration procedure, simulations have been performed by considering weak perturbations of the IR driving pulse and by allowing the iteration procedure to run

until a convergence of the fitness function is obtained. In the simulations shown in Figure 6, the first iteration has been performed by scanning the attenuation parameter from $\alpha = 10^9$ to $\alpha = 10^{10}$ in steps of $\Delta\alpha = 5 \times 10^8$, and the angular position has been scanned from $\theta = -720^\circ$ to $\theta = 720^\circ$ in steps of $\Delta\theta = 2^\circ$. The optimal values of the fitness parameters from the first iteration in this case are $\alpha = 10^9$ and $\theta = 466^\circ$, and $\chi^2 = 0.6789$. Once the optimal values have been determined from the first iteration, further iterations are performed by scanning only near the first iteration optimal region, which substantially improves the performance of the iterative method. In the present simulation the value of the fitness function converges at approximately the 5th iteration. The optimal values of the fitness parameters from the 5th iteration are $\alpha = 10^{10}$ and $\theta = 496^\circ$, and the value of the fitness function is $\chi^2 = 0.4927$. In Figure 6a the spectral amplitudes that result from the first and 5th iterations are shown. As it can be observed, the effect of the XUV pulses on the spectral amplitude is readily small, which is expected since the perturbation of the IR pulse is weak ($\alpha = 10^9 - 10^{10}$). The intensity of the optimal XUV pulse after the 5th iteration is shown in Figure 6b, and the inset shows the evolution of the value of the normalized χ^2 function for the increasing iterations. Clearly, as the iteration procedure evolves, the value of the fitness function improves such that at the 5th iteration an optimal compressed pulse is achieved. As shown in the inset of Figure 6b, the value of the normalized χ^2 function becomes basically constant after the 5th iteration, and therefore no substantial improvements are achieved by considering further iterations. This simulation therefore shows the robustness of the control method, which is able to achieve optimal fitness targets both by using relatively weak perturbations of the IR driving pulse with a single iteration and by considering very weak perturbations in a multiple iteration procedure.

Figure 5. (color online) Time-frequency analysis of the original (a) and optimized (b) spectra, for the case shown in Figure 4.

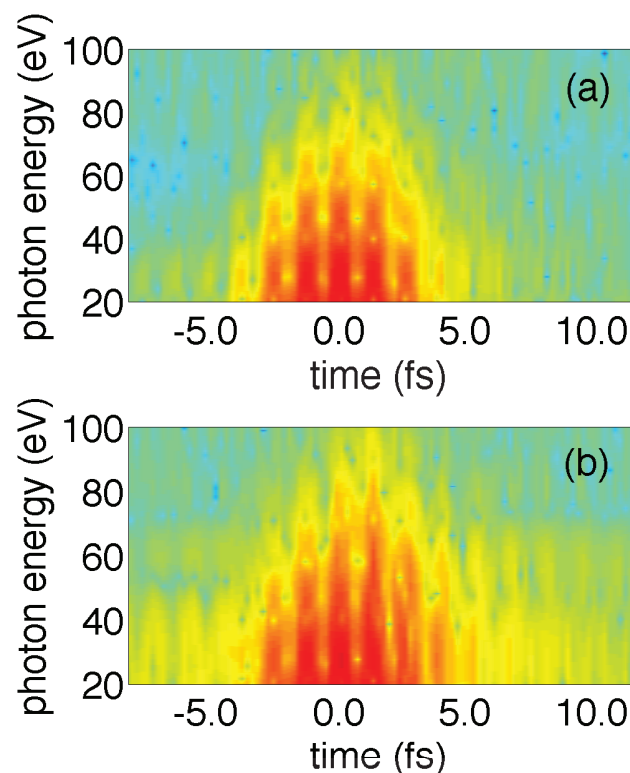
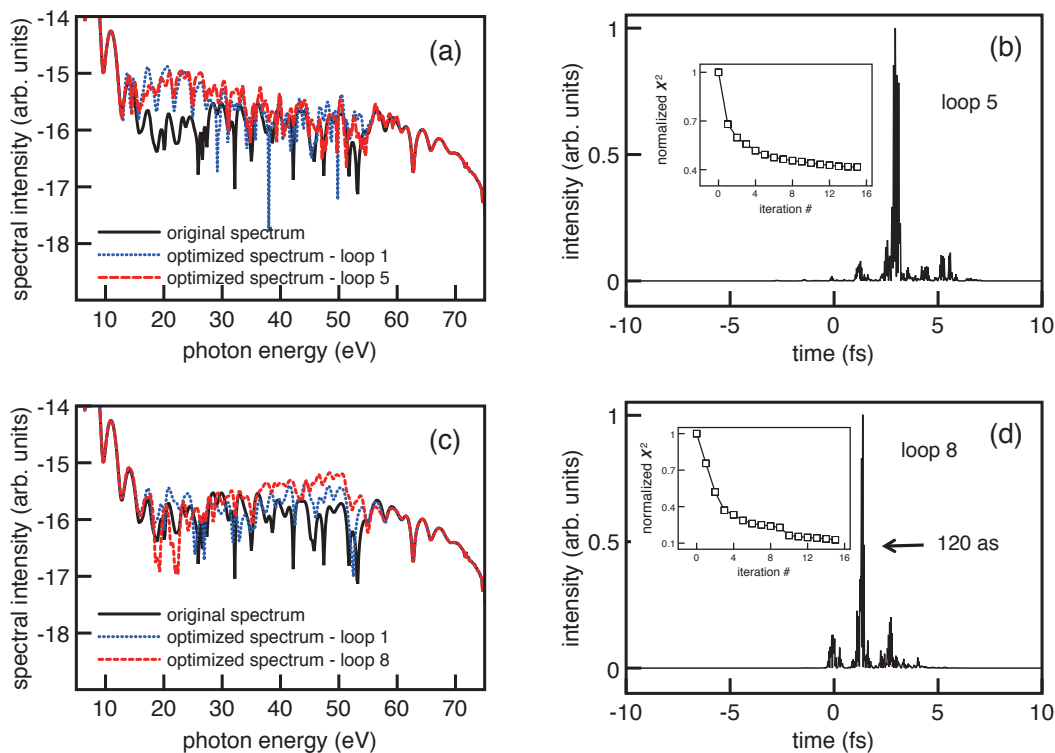


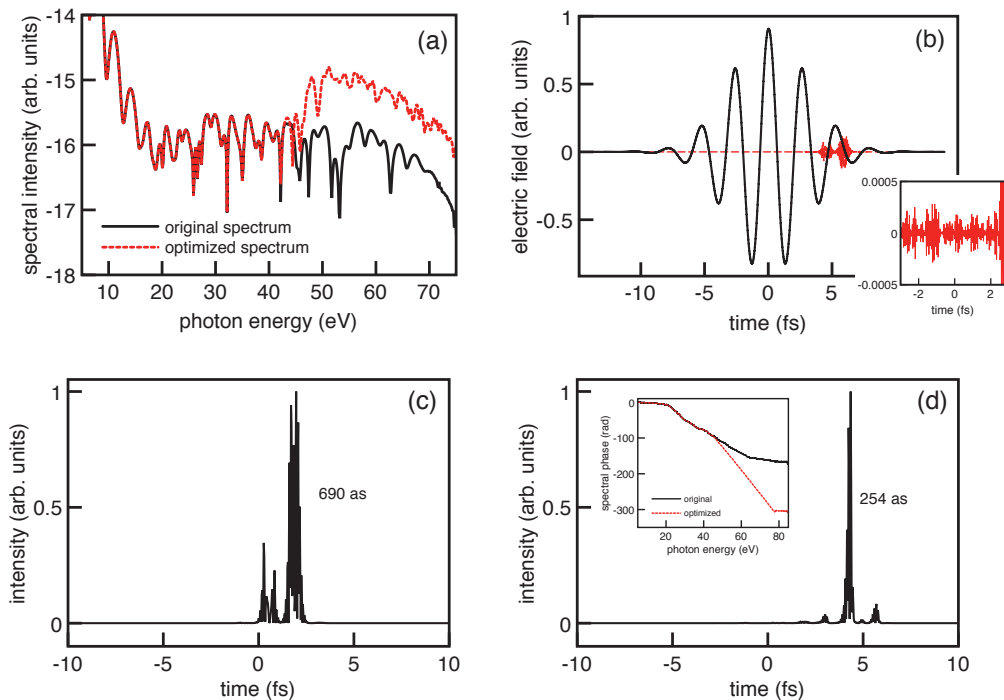
Figure 6. (Color online) Optimization of the HHG spectral region 21–51 eV obtained by considering several iterations of the feedback loop for α scanned from $\alpha = 10^9$ to $\alpha = 10^{10}$ (**a,b**) and from $\alpha = 10^{11}$ to $\alpha = 10^{12}$ (**c,d**). (**a,b**): The scan in the first iteration in θ is from $\theta = -720^\circ$ to $\theta = 720^\circ$. In the subsequent iterations, θ is scanned from $\theta = 200^\circ$ to $\theta = 700^\circ$. In (**a**) the spectral intensity of the original and optimized spectra are shown for the first and 5th iterations, as indicated. The optimal values of the fitness parameters for the 5th iteration are in this case $\alpha = 10^{10}$ and $\theta = 496^\circ$. In (**b**) the temporal evolution of the intensity of the XUV pulse resulting from the second interaction region after the 5th iteration (loop) is shown. The inset in (**b**) shows the value of the normalized χ^2 parameter as a function of the iteration number. From approximately the 5th iteration the value of χ^2 and the intensity profile of the resulting XUV pulse do not change substantially. (**c**) and (**d**): The scan in the all the iterations in θ is from $\theta = -720^\circ$ to $\theta = 720^\circ$. In (**c**) the spectral intensity of the original and optimized spectra are shown for the first and 8th iterations, as indicated. The optimal values of the fitness parameters for the 8th iteration are in this case $\alpha = 10^{12}$ and $\theta = 365^\circ$. In (**d**) the temporal evolution of the intensity of the XUV pulse resulting from the second interaction region after the 8th iteration is shown, which is an isolated single cycle pulse centered at 36 eV. The inset in (**d**) shows the value of the normalized χ^2 parameter as a function of the iteration number. From approximately the 8th iteration, the duration of the intensity profile of the resulting central XUV pulse does not change substantially. Note that the labels in the vertical axis of (**a**) and (**c**) indicate a logarithmic scale.



From the simulations that have been carried out, it can in general be concluded that the optimized configuration is not critically sensitive to the value of the intensity of the XUV₁ pulse, and also that

weak perturbations of the IR pulse seem to be generally more effective. This supports the fact that the short trajectories contribute most on the optimal configuration, since they are more robust against changes in the intensity compared with the long trajectories [2]. In order to compare the effect of a weaker XUV field on the iterative procedure, the previous simulations have been repeated by scanning the attenuation parameter from $\alpha = 10^{11}$ to $\alpha = 10^{12}$ in steps of $\Delta\alpha = 5 \times 10^{11}$. The corresponding results are shown in Figure 6c,d. Clearly, the iterative procedure is more effective by *gently* perturbing the IR field, achieving in this case an isolated single cycle pulse of 120 as at a central photon energy of 36 eV. Weaker XUV intensities have been computed with no further improvements of the optimization in this case.

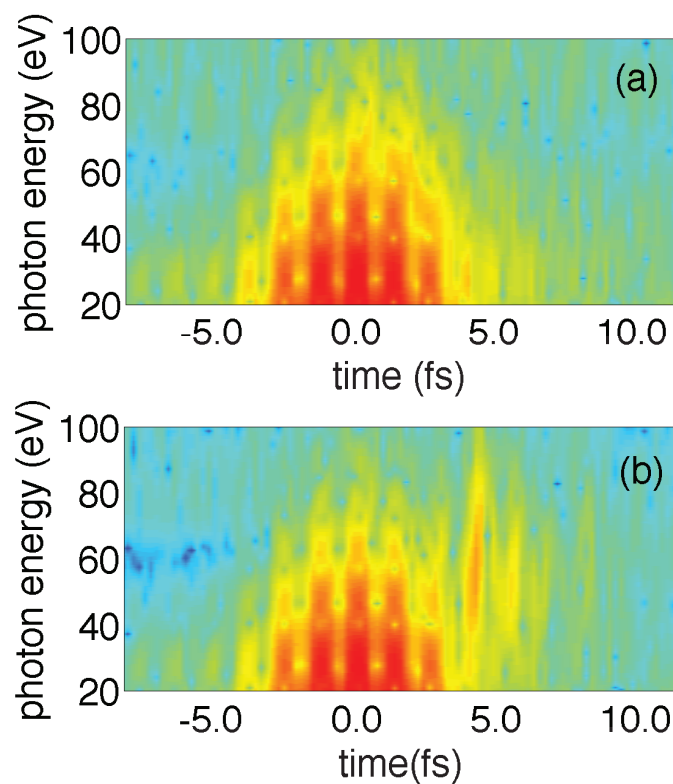
Figure 7. (Color online) Optimization of the HHG spectral region 50–70 eV obtained by considering a single feedback loop. The scan in θ is from $\theta = -720^\circ$ to $\theta = 720^\circ$, and α is scanned from $\alpha = 10^7$ to $\alpha = 10^8$. The value of the normalized χ^2 function is 0.8771 for the original spectrum and 0.2309 for the optimized one. In (a) the spectral intensity of the original and optimized spectra are shown, as indicated. The IR driving pulse together with the optimal XUV pulse are shown in (b). The amplitude of the IR pulse is normalized, and the one corresponding to the XUV pulse has been rescaled to allow its visualization. In this case the optimal values of the fitness parameters are $\alpha = 10^8$ and $\theta = 550^\circ$. (c,d) show the temporal evolution of the intensities of the XUV pulses resulting from the second interaction region, before and after optimization, respectively, which are centered at a photon energy of 60 eV. The inset in (d) shows the spectral phase for the original and optimized spectra. Note that the labels in the vertical axis of (a) indicate a logarithmic scale.



Finally, the optimization of the spectral amplitude has also been considered in a spectral region near the cutoff, as a second significative example, which shows the generality of the control technique. The filtered spectral region in this case is centered at 60 eV with a bandwidth of 20 eV, and the results are

shown in Figure 7. The numerical algorithm considers only a single feedback loop and scans from $\alpha = 10^7$ to $\alpha = 10^8$, in steps of $\Delta\alpha = 10^7$, and from $\theta = -720^\circ$ to $\theta = 720^\circ$, in steps of $\Delta\theta = 10^\circ$. The optimal values obtained in this case are $\alpha = 10^8$ and $\theta = 550^\circ$. Figure 7a shows how the spectral intensity is modified basically near the cutoff, *i.e.*, in the spectral region that is to be optimized. As in the case analyzed in Figure 2, where the optimization was considered for a region well in the plateau, the optimal position of the XUV₁ pulse with respect to the IR driving pulse lies near the late temporal wing, as shown in Figure 7b. As a result of this optimization procedure, the XUV original radiation from the second gas target, which includes a central pulse of ≈ 690 as (Figure 7c), is compressed to an isolated attosecond pulse of only 254 as, as shown in Figure 7d. The inset in Figure 7d shows how the phase of the spectrum is strongly modified due to the early wing of the XUV₁ pulse—the corresponding field amplitude is shown in the inset of Figure 7b, which induce a suppression of the yield generated around the central part of the IR pulse, as it was also observed in the case of Figures 2 and 3. Finally, the time-frequency analysis for the case near the cutoff is shown in Figure 8. As in the simulations commented previously, a yield enhancement can be observed in the late wing region of the IR field where the XUV₁ optimal pulse is centered, clearly showing again a selection of the short trajectories around the HHG region that is being optimized (50–70 eV).

Figure 8. (Color online) Time-frequency analysis of the original (a) and optimized (b) spectra, for the case shown in Figure 7.



4. Conclusions

In conclusion, a feedback loop scheme has been proposed for shaping the spectral amplitude in a broad spectral region of HHG. In previous results, it was shown that the same control technique is suitable to reshape the spectral phase in a broad region of the spectrum [20]. The technique is based on the combination of the IR intense driving pulse with the weak signal produced by the HHG process in a selected spectral bandwidth and can be applied in an iterative procedure. The success of the method is determined by the resolution of the scan in the intensity of the XUV pulses and their delay with respect to the IR pulse. For the simulations reported in the present study, the optimization of the spectral amplitude is found to be robust by considering variations of the optimal XUV pulse intensity of 20% and for a resolution of $\Delta\theta = 5^\circ$ (i.e., for a spatial resolution of ≈ 11 nm or a temporal delay resolution of ≈ 37 as). Also, the numerical algorithm that has been used in the present study represents the simplest numerical configuration, which has been chosen in order to demonstrate the capabilities of the method in the simplest case. Other possibilities including some genetic or evolutionary-type schemes are being tested. It has been thus demonstrated numerically that the radiation produced by HHG can be successfully used in a feedback loop scheme to weakly perturb the IR intense driving pulse so that optimal shapes of the spectral phase and amplitude can be achieved in a broad region of the spectrum. Using a single iteration (loop), isolated attosecond pulses have been obtained at different central photon energies by optimizing the spectral phase [20] or the spectral amplitude in the present paper, which shows the feasibility of the control technique in relatively simple experimental setups. The use of additional feedback loops allows to further optimize the final solution in some cases. This control tool can be readily applied to obtain other spectral phase and amplitude shapes different from the ones considered in the present study, and also considering higher photon energies, as, e.g., for the coherent control in the X-ray region, with the possibility to shape and achieve much shorter or also longer pulses.

Acknowledgments

Support from the Spanish Ministry of Economy and Competitiveness through “Plan Nacional” (FIS2011-30465-C02-02) is acknowledged.

References

1. Rabitz, H.; de Vivie-Riedle, R.; Motzkus, M.; Kompa, K. Whither the future of controlling quantum phenomena? *Science* **2000**, *288*, 824–828.
2. Agostini, P.; DiMauro, L.F. The physics of attosecond light pulses. *Rep. Prog. Phys.* **2004**, *67*, 813–855.
3. Scrinzi, A.; Ivanov, M.Y.; Kienberger, R.; Villeneuve, D.M. Attosecond physics. *J. Phys. B* **2006**, *39*, R1–R37.
4. Hentschel, M.; Kienberger, R.; Spielmann, C.; Reider, G.A.; Milosevic, N.; Brabec, T.; Corkum, P.; Heinzmann, U.; Drescher, M.; Krausz, F. Attosecond metrology. *Nature (London)* **2001**, *414*, 509–513.

5. Kienberger, R.; Hentschel, M.; Uiberacker, M.; Spielmann, C.; Kitzler, M.; Scrinzi, A.; Wieland, M.; Westerwalbesloh, T.; Kleinberg, U.; Heinzmann, U.; *et al.* Steering attosecond electron wave packets with light. *Science* **2002**, *297*, 1144–1148.
6. Kienberger, R.; Goulielmakis, E.; Uiberacker, M.; Baltuska, A.; Yakovlev, V.; Bammer, F.; Scrinzi, A.; Wieland, M.; Westerwalbesloh, T.; Kleinberg, U.; *et al.* Atomic transient recorder. *Nature (London)* **2004**, *427*, 817–821.
7. Lappas, D.G.; L’Huillier, A. Generation of attosecond xuv pulses in strong laser-atom interactions. *Phys. Rev. A* **1998**, *58*, 4140–4146.
8. Sansone, G.; Benedetti, E.; Calegari, F.; Vozzi, C.; Avaldi, L.; Flammini, R.; Poletto, L.; Villoresi, P.; Altucci, C.; Velotta, R.; *et al.* Isolated single. Cycle attosecond pulses. *Science* **2006**, *314*, 443–446.
9. Pfeifer, T.; Gallmann, L.; Abel, M.J.; Neumark, D.M.; Leone, S.R. Single attosecond pulse generation in the multicycle-driver regime by adding a weak second-harmonic field. *Opt. Lett.* **2006**, *31*, 975–977.
10. Pfeifer, T.; Gallmann, L.; Abel, M.J.; Nagel, P. M.; Neumark, D.M.; Leone, S.R. Heterodyne mixing of laser fields for temporal gating of high-order harmonic generation. *Phys. Rev. Lett.* **2006**, *97*, 163901:1–163901:4.
11. Chang, Z. Chirp of the single attosecond pulse generated by a polarization gating. *Phys. Rev. A* **2005**, *71*, 023813:1–023813:6.
12. Chang, Z. Controlling attosecond pulse generation with a double optical gating. *Phys. Rev. A* **2007**, *76*, 051403:1–051403:4.
13. López-Martens, R.; Varjú, K.; Johnsson, P.; Mauritsson, J.; Mairesse, Y.; Salières, P.; Gaarde, M.B.; Schafer, K.J.; Persson, A.; Svanberg, S.; *et al.* Amplitude and phase control of attosecond light pulses. *Phys. Rev. Lett.* **2005**, *94*, 033001:1–033001:4.
14. Abel, M.J.; Pfeifer, T.; Nagel, P.M.; Boutu, W.; Bell, M.J.; Steiner, C.P.; Neumark, D.M.; Leone, S.R. Isolated attosecond pulses from ionization gating of high-harmonic emission. *Chem. Phys.* **2009**, *366*, 9–14.
15. Feng, X.; Gilbertson, S.; Mashiko, H.; Wang, H.; Khan, S.D.; Chini, M.; Wu, Y.; Zhao, K.; Chang, Z. Generation of isolated attosecond pulses with 20 to 28 femtosecond lasers. *Phys. Rev. Lett.* **2009**, *103*, 183901:1–183901:4.
16. Naumova, N.M.; Nees, J.A.; Sokolov, I.V.; Hou, B.; Mourou, G.A. Relativistic generation of isolated attosecond pulses in a λ^3 focal volume. *Phys. Rev. Lett.* **2004**, *92*, 063902:1–063902:4.
17. Raith, P.; Ott, C.; Pfeifer, T. Attosecond twin-pulse control by generalized kinetic heterodyne mixing. *Opt. Lett.* **2011**, *36*, 283–285.
18. Winterfeldt, C.; Spielmann, C.; Gerber, G. Optimal control of high-harmonic generation. *Rev. Mod. Phys.* **2008**, *80*, 117–140.
19. Kholer, M.C.; Pfeifer, T.; Hatsagortsyan, K.Z.; Keitel, C.H. Frontiers of atomic high-harmonic generation. *Adv. At. Mol. Opt. Phys.* **2012**, *61*, 159–208.
20. Serrat, C. Broadband spectral phase control in high-order harmonic generation. *Phys. Rev. A* **2012**, submitted for publication.

21. Ishikawa, K. Photoemission and ionization of He⁺ under simultaneous irradiation of fundamental laser and high-order harmonic pulses. *Phys. Rev. Lett.* **2003**, *91*, 043002:1–043002:4.
22. Schafer, K.J.; Gaarde, M.B.; Heinrich, A.; Biegert, J.; Keller, U. Strong field quantum path control using attosecond pulse trains. *Phys. Rev. Lett.* **2004**, *92*, 023003:1–023003:4.
23. Gaarde, M.B.; Schafer, K.J.; Heinrich, A.; Biegert, J.; Keller, U. Large enhancement of macroscopic yield in attosecond pulse train-assisted harmonic generation. *Phys. Rev. A* **2005**, *72*, 013411:1–013411:7.
24. Takahashi, E.J.; Kanai, T.; Ishikawa, K.L.; Nabekawa, Y.; Midorikawa, K. Dramatic enhancement of high-order harmonic generation. *Phys. Rev. Lett.* **2007**, *99*, 053904:1–053904:4.
25. De Morisson Faria, C.F.; Salières, P. High-order harmonic generation with a strong laser field and an attosecond-pulse train: The Dirac-delta comb and monochromatic limits. *Laser Phys.* **2007**, *17*, 390–400.
26. Fleischer, A.; Moiseyev, N. Amplification of high-order harmonics using weak perturbative high-frequency radiation. *Phys. Rev. A* **2008**, *77*, 010102:1–010102:4.
27. Seres, J.; Yakovlev, V.S.; Seres, E.; Streltsov, C.; Wobrowski, P.; Spielmann, C.; Krausz, F. Coherent superposition of laser-driven soft-X-ray harmonics from successive sources. *Nat. Phys.* **2007**, *3*, 878–883.
28. Press, W.H.; Teukolsky, S.A.; Vetterling, W.T.; Flannery, B.P. *Numerical Recipes: The Art of Scientific Computing*; Cambridge University Press: Cambridge, UK, 2007.
29. Lewenstein, M.; Balcou, P.; Ivanov, M.Y.; L’Huillier, A.; Corkum, P.B. Theory of high-harmonic generation by low-frequency laser fields. *Phys. Rev. A* **1994**, *49*, 2117–2132.

© 2012 by the author; licensee MDPI, Basel, Switzerland. This article is an open access article distributed under the terms and conditions of the Creative Commons Attribution license (<http://creativecommons.org/licenses/by/3.0/>).